



Quantitative evaluation of the uncertainty sources for the modeling of atmospheric CO₂ concentration within and in the vicinity of Paris city

Jinghui Lian¹, François-Marie Bréon¹, Grégoire Broquet¹, Bo Zheng¹, Michel Ramonet¹, and Philippe Ciais¹

¹Laboratoire des Sciences du Climat et de l'Environnement (LSCE), IPSL, CEA-CNRS-UVSQ, Université Paris-Saclay, Gif-sur-Yvette, France

Correspondence to: Jinghui Lian (Jinghui.Lian@lsce.ipsl.fr)

Abstract. The top-down atmospheric inversion method that couples atmospheric CO₂ observations with an atmospheric transport model has been used extensively to quantify CO₂ emissions from cities. However, the potential of the method is limited by several sources of misfits between the measured and modeled CO₂ that are of different origins than the targeted CO₂ emissions. This study investigates the critical sources of errors that can compromise the estimates of the city-scale emissions and identifies the signal of emissions that has to be filtered when doing inversions. A set of one-year forward simulations is carried out using the WRF-Chem model at a horizontal resolution of 1 km focusing on the Paris area with different anthropogenic emission inventories, physical parameterizations and CO₂ boundary conditions. The simulated CO₂ concentrations are compared with in situ observations from six continuous monitoring stations located within Paris and its vicinity. Results highlight large nighttime observation-model misfits, especially in winter within the city, which are attributed to large uncertainties in the diurnal profile of anthropogenic emissions as well as to errors in the vertical mixing near the surface in the WRF-Chem model. The nighttime biogenic respiration to the CO₂ concentration is a significant source of modeling errors during the growing season outside the city. When winds are from continental Europe and the CO₂ concentration of incoming air masses is influenced by remote emissions and large-scale biogenic fluxes, differences in the simulated CO₂ induced by the two different boundary conditions (CAM5 and CarbonTracker) can be of up to 5 ppm. Our results suggest three selection criteria for the CO₂ data to be assimilated for the inversion of CO₂ emissions from Paris (i) discard data that appear as statistical outliers in the model-data misfits which are interpreted as model's deficiencies under complex meteorological conditions; (ii) use only afternoon urban measurements in winter and suburban ones in summer; (iii) test the influence of different boundary conditions in inversions. If possible, using additional observations to constrain the boundary inflow, or using CO₂ gradients of upwind-downwind stations, rather than absolute CO₂ concentration, as atmospheric inversion inputs.

1 Introduction

Worldwide, almost two-thirds of global final energy consumption takes place in urban agglomeration areas that have a high population density and corresponding infrastructure, and cities are responsible for more than 70% of the global anthropogenic CO₂ emissions (IEA, 2016; Seto et al., 2014). Due to progressing urbanization processes, the number of people living in cities is expected to increase from the current 7.7 billion in 2019 to more than 9.7 billion by 2050 (United Nations, 2019). More than ever, cities are at the front line of climate change mitigation and take the lead in energy transition and emission reduction of greenhouse gases.

Currently, a variety of efforts are underway to quantify cities' total CO₂ emissions and establish a high spatially and temporally resolved emission inventory for supporting urban emission mitigation strategies. An independent monitoring of city emission is highly desirable, which could be delivered by the top-down atmospheric inversion method using regional high-resolution transport models together with ground-based urban CO₂ concentration networks and/or satellites with imagery capabilities. The so-called



atmospheric inversion provides an optimized estimate of CO₂ emissions aiming at the best agreement between atmospheric CO₂ measurements and their simulated equivalents. It relies on the filtering of the CO₂ signal associated with the urban emissions at the targeted spatial and temporal scales from other sources of misfits between measured and modeled CO₂ concentrations. These other sources of misfits include uncertainties in the atmospheric transport, in atmospheric CO₂ conditions that are used at the boundaries of the regional model, in the natural CO₂ fluxes within the modeling domain, but also in the spatial and temporal distribution of the urban emissions at scales finer than the targeted ones. Even when controlling the emissions at a relatively high temporal and spatial resolution, city-scale inversion frameworks have generally targeted monthly to annual budgets of the emissions at the city scale, or for large areas of these cities (strong temporal and spatial correlations are assumed). The uncertainties in the assumed temporal and spatial emission variations induce a critical source of error poorly constrained by the inversions due to the lack of data (Brón et al. 2015; Lauvaux et al. 2016). The spatial and temporal allocation of the emissions is generally derived from high-resolution gridded inventory based on uncertain activity data in the transportation, residential, and power sectors (Gately et al., 2017). Moreover, local sources of CO₂ emission in the vicinity of an urban station can cause variations of atmospheric CO₂ that are not captured by the inventories and transport models of kilometric scale that have been used for city inversions so far (Boon et al., 2016; Lian et al., 2019). Further, cities have green areas and are surrounded by rural areas that actively take up CO₂ in the daytime during the growing season. Uncertainties and variability in those biogenic fluxes also significantly affect the results of atmospheric inversions (Hardiman et al., 2017).

Uncertainties in modeling the atmospheric transport of CO₂ are exacerbated in urban areas due to building obstacles that generate specific mixing processes and modify the wind speed and direction. In addition, sensible heat emissions at the surface of urban areas enhance vertical mixing, increase the depth of the boundary layer (Dupont et al., 1999) and can drive regional mesoscale circulations under certain conditions. To reduce transport uncertainties in inversions over urban areas, one can use dedicated urban surface schemes (e.g. Nehr Korn et al., 2013; Feng et al., 2016). More general approaches to reduce transport errors rely on the assimilation of upper-air weather data or on the optimization of the model configuration, e.g. based on comparisons against independent wind measurements (e.g. Deng et al., 2017). But some errors remain difficult to quantify, such as those from local circulations and complex meteorological conditions (Martin et al., 2019). As a consequence, an empirical selection of the data to be assimilated is usually performed, which is more or less stringent depending on each urban station and transport model. Typical selection criteria of continuous urban CO₂ data consist of (i) using only measurements acquired during the afternoon when a well-developed convective mixing layer is expected; (ii) using only observations when the wind speed is above a given threshold; (iii) removing statistical outliers.

Uncertainties in CO₂ boundary conditions arise from the fact that city-scale inversions are performed over a limited spatial domain that receives CO₂ signals from outside. These boundary conditions usually cannot be measured explicitly and they can be complex for continental cities that receive CO₂ advected by long-range and middle-range transport from other urban areas and biogenic fluxes. Göckede et al. (2010) found that small biases in CO₂ boundary condition could lead to large errors (~47%) in the posterior annual state-level CO₂ fluxes of Oregon. Lauvaux et al. (2012) found that a 0.55 ppm bias of CO₂ boundary condition induced a 10% bias in the posterior annual CO₂ flux of Iowa and surrounding states. In order to try to eliminate the bias from boundary conditions, Brón et al. (2015) and Staufer et al. (2016) proposed to assimilate CO₂ gradients between upwind-downwind stations in inversions of CO₂ fluxes of the Paris area, which reduces the number of data that can be assimilated.

Series of CO₂ transport and inverse modeling studies have been conducted for Paris (Brón et al., 2015; Staufer et al., 2016; Wu et al., 2016; Broquet et al., 2018; Xueref-Remy et al., 2018). A network of seven stations, including two stations at the center of the city and five stations in its vicinity, has been maintained since 2014. This study resumes this activity and aims at supporting the revisit of some of the options previously used for the inversion based on a more advanced transport modeling framework



developed by Lian et al. 2018 and 2019. More specifically, we analyze in detail the model-measurement mismatches so as to identify critical sources of errors that would compromise a high-resolution atmospheric inversion of urban CO₂ emissions in the Paris area. A set of forward simulations of atmospheric CO₂ concentration are performed at 1-km horizontal resolution using the WRF-Chem model (Grell et al., 2005) with different anthropogenic emission inventories, physical parameterizations and CO₂ boundary conditions over the Paris region from December 2015 to November 2016. The main objective of this paper is to describe and quantify the uncertainties induced by anthropogenic emissions, biogenic fluxes, atmospheric transport and CO₂ boundary conditions. We also address the question to what extent these model-measurement mismatches might be reduced and how our proposed diagnostics could be used to provide additional constraints for the inversion of CO₂ emissions at the city scale.

2 Methods

2.1 Experimental design

The WRF-Chem V3.9.1 model was used to simulate hourly atmospheric CO₂ concentrations over the Paris region. Details regarding the model setup and the reference data used in the simulations are outlined briefly below and described in Lian et al. (2019). The model was configured with one-way nesting of three modeling domains (D01, D02, and D03 in Figure 1a) at horizontal grid resolutions of 25, 5 and 1 km respectively, in which the innermost one (D03) covers the Île-de-France region (IdF, which is the administrative area that includes the Paris urban area) and its surrounding. The meteorological initial and lateral boundary conditions were retrieved from the global European Centre for Medium-Range Weather Forecasts (ECMWF) Interim Re-Analysis data (ERA-Interim) with 0.75°×0.75° horizontal resolution at 6-hourly update intervals (Berrisford et al., 2011). The grid nudging option in WRF to relax the model to ERA-Interim on large scales was applied to temperature and wind fields at model levels above the planetary boundary layer (PBL) of the outer two domains. We also used the surface analysis nudging and observation nudging options to assimilate the National Centers for Environmental Prediction (NCEP) operational global upper-air (ds351.0) and surface (ds461.0) observation weather station data (<https://rda.ucar.edu/datasets/ds351.0/>; <https://rda.ucar.edu/datasets/ds461.0/>), which are described in more detail in Lian et al. (2018). The biogenic CO₂ fluxes were calculated online in WRF-Chem by the diagnostic biosphere Vegetation Photosynthesis and Respiration Model (VPRM) (Mahadevan et al., 2008; Ahmadov et al., 2007, 2009).

2.1.1 Atmospheric physics options

An accurate physical parameterization of atmospheric transport model is critical to numerical simulations of the meteorology and CO₂ concentrations within and around urban areas. A set of numerical experiments was performed to assess the sensitivity of the simulations with the WRF-Chem model to the choice of different physics schemes. The characteristics of CO₂ distributions are highly related to the PBL structure and its temporal evolution. We thus carried out sensitivity experiments with three different PBL parameterization schemes (Table 1a), including the Yonsei University scheme (YSU) (Hong et al., 2006), the Mellor-Yamada-Janjic scheme (MYJ) (Janjić, 1990, 1994), and the Bougeault-Lacarrère scheme (BouLac) (Bougeault and Lacarrere, 1989). In addition, two different urban surface parameterizations were investigated, the single-layer urban canopy model (UCM) (Chen et al., 2011) and the multilayer urban canopy model BEP (Building Effect Parameterization) (Martilli et al., 2002) (Table 1a). The non-local YSU scheme was used with the Revised MM5 Monin-Obukhov surface layer scheme (Jiménez et al., 2012), whereas the two local MYJ and BouLac schemes were used with the Monin-Obukhov Eta Similarity surface layer scheme (Janjić, 1996). All other physics options were identical for all sensitivity runs: WSM6 microphysics scheme (Hong and Lim, 2006), RRTM longwave radiation scheme (Mlawer et al., 1997), Dudhia shortwave radiation scheme (Dudhia, 1989), Unified Noah land-surface scheme for non-urban land cover surface energy fluxes (Chen and Dudhia, 2001). The Grell 3D ensemble cumulus convection



scheme (Grell and Déry, 2002) was only employed for the outer domain (D01). These options correspond to those selected by Lian et al. (2018) which showed good performances for simulating near-surface winds and temperatures over the Paris region. The simulations were performed for a period of 15 months from September 2015 to November 2016 including a spin-up of three months.

2.1.2 Anthropogenic emission inventories

5 Numerical experiments were carried out to assess the modeled CO₂ sensitivity to the use of different anthropogenic emission maps and to get insights on the signature of typical uncertainties in such maps (Table 1b). The two spatially and temporally explicit emission fields derived from inventories used in this study were the 2010 AirParif inventory at a spatial resolution of 1 km (AIRPARIF, 2013) and the European greenhouse gas emission inventory (5 km × 5 km resolution) for the base year 2005 developed by the Institute of Economics and the Rational Use of Energy (IER), University of Stuttgart (<http://carboeurope.ier.uni-stuttgart.de/>). Both inventories simulated monthly, weekly and diurnal profiles and were rescaled on the basis of the ratios of the national annual budgets of CO₂ emissions for the countries within the domain, between the base year and the year of simulation (2015/2016), taken from Le Quéret et al. (2018).

10 Figures 1b and 1c show a map of daily CO₂ emission within the IdF region for a weekday in November 2015 from the 1-km AirParif inventory and the 5-km IER inventory respectively. The figures show that the emissions are the largest within and in the near vicinity of the Paris administrative city (the core of the urban area). The suburban area extends approximately 15 km outside of the city limits. The AirParif inventory is expected to offer a more robust description of the emissions for the year of simulation than the IER inventory does because it uses more local and more recent data (AIRPARIF, 2013).

15 The temporal variations of emissions also show some differences, in particular when differentiated per sector (Figure 2). The emissions, split up by five sectors (namely building, surface traffic, energy, industry, and all other sectors), are different both in terms of magnitude and diurnal cycle between the two inventories. This is true both for the very center of Paris where the CDS CO₂ measurement station is located (Figure 2a) and on a relatively large (5-km) spatial scale (Figure 2b). The relative difference between the two inventories is smaller in terms of total emissions. Figures 2c and 2d show the total emission for both IER and AirParif inventories as a function of time in the day. At the larger scale (Figure 2d), a substantial difference is found during the early morning when AirParif shows emissions that are much smaller than those of IER, and with a clear temporal trend.

20 We made a one-month simulation using these two anthropogenic inventories together with their respective temporal profiles in order to analyze the impact on the simulated CO₂ concentrations (Table 1b). Within the same group of simulations, we also used (i) a constant temporal profile (each pixel has a different emission, but constant in time based on the temporal average of the AirParif inventory) and (ii) a constant and spatially homogeneous emission where the emissions are distributed uniformly over the IdF whole territory. Distinct CO₂ tracers are used for each of the four experiments to quantify their respective impacts on the atmospheric CO₂ concentration, for a given configuration of the WRF-Chem model. The simulation was carried out for the one-month period of January 2016 when the influence of regional biogenic flux on CO₂ signals is relatively small compared to that of anthropogenic flux.

2.1.3 Boundary conditions for CO₂

35 A set of sensitivity experiments was designed to investigate the impact of different CO₂ boundary conditions on the Paris CO₂ concentrations (Table 1c). The initial and lateral boundary conditions for CO₂ concentration fields used in the sensitivity experiments were taken from two global CO₂ atmospheric inversion products at 3-hourly update intervals: CAMS and CarbonTracker. CAMS has a horizontal resolution of 3.75° × 1.90° (longitude × latitude), with 39 hybrid layers in the vertical (version v16r1, <https://apps.ecmwf.int/datasets/data/cams-ghg-inversions/>; Chevallier, 2017a, 2017b). CarbonTracker has a



horizontal resolution of 3° in longitude and 2° in latitude, with 25 vertical layers (version CT2017, <http://carbontracker.noaa.gov>; Peters et al. 2007). Both global datasets were interpolated onto the outermost domain of WRF-Chem (D01) (bilinearly in longitude, longitude and linearly in pressure) so as to provide the lateral boundary conditions for CO_2 simulations. Given that CarbonTracker has an averaged value over each 3-hourly interval (the times on the date axis are the centers of each averaging period), it was also

5 linearly interpolated in time to ensure consistency with both CAMS and the interval of input data for WRF-Chem (e.g. the value at 00 UTC was generated by interpolating the one at 22.5 UTC of the previous day with the one at 1.5 UTC of the same day).

Figure 3 shows time series of average differences in CO_2 concentration between CAMS and CarbonTracker at each of the four lateral boundaries, averaged over the lowest 0.7 km above ground level (AGL), of D01 for both 00 UTC and 12 UTC. These time series are the spatial mean and standard deviation ($\pm 1\sigma$) over each boundary (a latitudinal transect for western and eastern boundaries / a longitudinal transect for southern and northern boundaries). In general, winds blow mostly from the west in all

10 seasons over the domain of interest. Small differences at the western boundary are observed under the influence of prevailing westerlies with annual means of the spatial mean and standard deviation of 0.01 ± 2.8 ppm for 00 UTC and 0.4 ± 1.8 ppm for 12 UTC, which is expected as the air masses are advected from clean air (oceanic) areas. In contrast, the differences are significantly larger at the eastern boundary (-4.8 ± 7.4 ppm for 00 UTC and -1.7 ± 3.3 ppm for 12 UTC), but can vary from day to day depending

15 on the synoptic weather condition. This feature indicates that CAMS and CarbonTracker may provide substantially different continental CO_2 background signals to the inner domain when the wind blows from the east. Moreover, the magnitude and variability of the differences are overall smaller at noon compared to those at midnight. The variability of nighttime differences appears relatively larger in summer than those in winter. Note that the CO_2 differences between CAMS and CarbonTracker are much smaller for the upper layers above 0.7 km AGL, with annual means of the spatial mean and standard deviation of -0.4 ± 0.4

20 ppm for both 00 UTC and 12 UTC at the eastern boundary (Figure S1).

The WRF-Chem simulation with boundary conditions from CarbonTracker used the same physics schemes and prior fluxes as the one with boundary conditions from CAMS (also defined as the control run), whereas it was only carried out for the parent domain (D01) without nesting over a full-year period (2015.09-2016.11). Given the fact that lateral boundary conditions are fed to the nested domain from the parent (the nest is driven along its lateral boundaries by the parent domain), results from D01 should

25 therefore be representative enough to access the modeled CO_2 sensitivity over the IdF region to the use of different CO_2 boundary conditions.

2.2 CO_2 in situ observations

For the model evaluation, we use observations from six in situ continuous CO_2 monitoring stations established in the IdF region. Four stations (AND, COU, OVS, SAC) are located within peri-urban areas and two (JUS and CDS) are located within the Paris

30 city. The SAC station has two air inlets placed at 15 m and 100 m AGL respectively. Each of the other stations is equipped with a continuous CO_2 gas analyzer and inlets located on rooftops or on towers with heights varying from 20 m to 60 m AGL. The CO_2 analyzers are high-precision cavity ring-down spectroscopy instruments with a calibration system using three reference gases tied to the WMO CO_2 X2007 scale every 2 to 6 months (Tans et al., 2011). The six stations within IdF are complemented by two ICOS atmospheric background CO_2 tall tower monitoring stations (TRN and OPE) located respectively 101 km and 235 km away from

35 the center of Paris. In this study, these two stations are only used as potential background sites and to provide additional support and validations for the results of diagnostics made at the SAC site. The locations of all the observing stations together with their sampling heights are shown in Figure 1.



3 Results

3.1 Overall model performance

In this section, we start with an evaluation of the overall performance of the control run (BEP_MYJ) in simulating atmospheric CO₂ over the full-year period. The accuracy of model estimates at the six in situ measurement stations is assessed using three statistical indicators corresponding to the hourly values: the correlation coefficient (R), the root mean square error (RMSE) and the mean bias error (MBE). We also use the K-nearest neighbors (KNN) algorithm with an outlier fraction of 0.1 (10%) to detect the largest model-observation mismatches so as to minimize their influences on the statistical results (Ramaswamy et al., 2000; Zhao et al., 2019). These large model-observation discrepancies may be due e.g. to the occasional contaminations from local sources of CO₂ emissions near the measurement station that cannot be resolved by the 1-km resolution model, or to the failure of the model in the description of CO₂ concentrations under some meteorological conditions such as heavy rains and storms, thick clouds with a thermodynamically stable inversion (diagnosed hereafter from Bulletin Climatique Météo-France, 2016).

Figure 4 shows, for the six monitoring sites, the scatter plots of the BEP_MYJ simulated vs. observed all hourly CO₂ concentrations from December 2015 to November 2016. The typical CO₂ concentrations vary between 390 and 430 ppm, and up to 440 ppm within the city (JUS and CDS stations). For short periods, the concentrations can be much higher (both for the observations and the model), in particular within the city where values of more than 500 ppm are sometimes observed. However, these data are considered as “outliers” by the KNN. When considering all data-points, the correlations vary between 0.5 for the JUS station at the very center of Paris to 0.76 at AND. The correlations get larger (0.55-0.83) when KNN outliers are removed. This correlation is partly driven by the seasonal cycle of CO₂ and does not provide specific information on the model’s ability to reproduce the short-term variations. The MBEs are of a few ppm, and at the OVS station can go up to -6 ppm. The KNN removal of outliers tends to reduce these biases, but not so within the Paris city. Finally, the RMSEs are larger than 10 ppm in most stations. RMSE values are significantly reduced through the KNN data selection but nevertheless range between approximately 5 and 10 ppm.

Figure 5 shows the average diurnal cycles split up by season for the measurements and the model results. It also shows the corresponding differences between the model and the data. These figures clearly show the seasonal variability with summer concentrations smaller than those during the rest of the year (due to photosynthetic absorption), larger concentrations within the city (JUS and CDS) (in the largest cluster of anthropogenic emissions), and the strong diurnal cycle that is mostly driven by atmospheric mixing. Both observations and the model show a double-peak pattern in the diurnal cycle of CO₂ concentrations at the two urban stations in winter. In addition to the mean seasonal cycle that is generated by large-scale (continental, hemispheric) vegetation photosynthetic uptake and respiration coupled to long-range transport, the variability of the synoptic-scale atmospheric flow also impacts the seasonal concentrations. It is worth noting that the CO₂ concentrations in autumn 2016 (SON) are on average higher than the other seasons, even slightly larger than those of the winter period (DJF) in 2015. This is interpreted as the consequence of persistent anticyclonic conditions leading to dry and calm weather over the north of France, and thus CO₂ accumulation near the surface throughout that period (Bulletin Climatique Météo-France, 2016).

The model reproduces the main features of the average diurnal cycle of CO₂ during the different seasons but the measurement-model discrepancies can be significant. At noon and during the afternoon, the mean differences are on the order of a ppm (with the exception of JUS). The model underestimates CO₂ with a time-varying bias roughly ranging from 0 to 12 ppm across stations for all seasons during the night until around 05 UTC. The two stations within the city have different behaviors, with larger differences, in particular the JUS station located at the city center. For this station, significant measurement-model discrepancies varying from 0 to 7 ppm over time are found, even during the afternoon when a good agreement is found at the other stations. Moreover, the model reproduces much smaller amplitudes of CO₂ diurnal cycle than the observations, in particular at the suburban stations.



The measurements themselves have an accuracy that is on the order of a fraction of a ppm (Xueref-Remy et al., 2018) and measurement errors are therefore negligible when analyzing such model-data differences. In the following, we analyze in further detail the measurement-model discrepancies and attempt to identify cases when they appear to be mainly driven by uncertainties in the anthropogenic emissions, in the biogenic fluxes, in the physical parameterizations of the atmospheric transport model, or in the CO₂ boundary conditions at the limit of the atmospheric transport model.

3.2 Contribution of main sources of errors in the simulated CO₂ related to different factors

3.2.1 Emission inventory

The main objective when measuring CO₂ concentrations within or in proximity to the city is to estimate the anthropogenic emissions by means of an atmospheric inversion. It is then natural to seek, in the time series, unambiguous signatures of erroneous assumptions on the anthropogenic emissions. This is a difficult task as significant uncertainties in the atmospheric transport also impact the modeling results, while there is no knowledge of both “true” emissions and “true” transport.

Figure 6 shows the results of the sensitivity experiments that used different temporal profiles and spatial distributions of anthropogenic CO₂ emissions (see Table 1b and Figure 2). The decomposition of the CO₂ concentration per tracer makes it very clear that the diurnal cycle of CO₂ at the six measurement sites is almost entirely associated with the signature of the anthropogenic emissions in January when the biogenic flux is small. This may not hold during the growing season. None of the simulations shows a diurnal cycle that is close to the observed one. The most striking error is the variation of the concentrations during the night with the observation showing an increase of CO₂ and the model showing a clear decrease. This simulated decrease is in part related to the emission that has a decreasing trend during the night (Figure 2). Indeed, when assuming an emission constant in time, the decreasing trend is reduced and the modeled value (green line in Figure 6) gets somewhat closer to the observation. Further analysis shows that the nighttime trend of the anthropogenic emission in January is mostly linked to residential heating in the inventory. The diurnal profile used for heating emissions in the AirParif inventory (with a significant decrease along the night) can thus be questioned.

Although there is a strong indication that the nighttime profile of the AirParif CO₂ emissions is erroneous and that heating emissions do not reduce strongly during the night, this error does not entirely explain the model-data misfit at CDS shown in Figure 6. This is proven by the fact that even the “constant emission” simulation does not reproduce the increasing concentration during the night. This implies that errors in atmospheric transport are also contributing to the model-data misfit, in particular concerning the vertical mixing near the surface. Further evidence for the transport deficiency is that the underestimations of nighttime CO₂ concentration are not only large at the two urban sites but also obvious at all rural stations (Figure 5).

To gain insights on vertical transport differences, we show in Figure 7 the vertical distribution of the BEP_MYJ modeled CO₂ concentrations at CDS in January together with time series of observed and simulated CO₂ concentrations at a sampling height of 34 m AGL. The PBL heights shown in Figure 7 are diagnosed using the 1.5-theta-increase method which defines the height of PBL as the level at which the potential temperature first exceeds the minimum potential temperature within the boundary layer by 1.5 K (Nielsen-Gammon et al., 2008). Results show that the model reproduces large vertical gradients in CO₂ concentrations in the low atmosphere levels, i.e. up to approximately 300 m AGL but mostly in the first 100 m. The largest concentrations are observed in low-wind conditions and when the PBL is shallow. It is worth noting that the modeled CO₂ concentrations within the PBL are not vertically homogeneous but exhibit a strong gradient. This indicates that when the measurements are under a strong influence of upwind emissions or close to the large sources of emissions, the mixing is far from complete, even during the afternoon.

Moreover, both the BEP_MYJ and BEP_MYJ_IER model slightly overestimate CO₂ concentrations at CDS in the late afternoon and early evening (from 18 pm to 22 pm) not only in January (Figure 6) but also over the full year (Figure 5). This is interpreted



as the consequence of a shift from a situation with convective mixing to stable nocturnal conditions around sunset occurring too early in the model. It may also be linked to an increase in traffic emissions during the evening rush hour, which could also lead to the overestimated modeled concentrations in the late afternoon.

3.2.2 Biogenic fluxes

5 To analyze the influence of biogenic fluxes on the CO₂ concentrations, we computed CO₂ horizontal differences between two sites (i) CDS, that is within the limits of the Paris city where the diurnal cycle in winter is dominated by anthropogenic emissions (see Figure 6) and (ii) SAC that is over a more rural area with a mix of crops and forest, so that the variations of CO₂ concentrations at that site are driven by biogenic fluxes in the domain and CO₂ background conditions. Figures 8a and 8b show the time series of the observed and BEP_MYJ simulated horizontal differences in near-surface daily CO₂ concentration between CDS and SAC for two different periods of the day, the afternoon mean (11-16 UTC) and the nighttime mean (21-05 UTC) from December 2015 to November 2016.

The separate tracers from the WRF-Chem model make it possible to quantify the respective contribution of anthropogenic, biogenic and background sources to the CO₂ difference between CDS and SAC (Figure 8c and 8d). During the afternoon, the CO₂ differences are mostly positive and result primarily from the larger contribution of the anthropogenic emissions at CDS, both during the growing and non-growing season. This result indicates that the magnitude of daytime net carbon uptake by plants does not fully offset that of the anthropogenic emissions, and thus the CO₂ concentration gradients between the upwind and downwind stations that are used in previous inversion studies (Brón et al., 2015; Stauffer et al., 2016) can also be used even during the growing season. During the night, there is a large measurement-model discrepancy from June to September (the SAC station had unfortunately measurement gaps). During this growing season period, the observed difference between CDS and SAC is negative at night (higher concentrations at SAC than at CDS), while the simulated difference is positive resulting from a large positive anthropogenic contribution and a smaller negative biogenic contribution. Figure S2 shows that this nighttime misfit between the modeled and observed CO₂ differences has a seasonal trend that follows closely the one of the modeled gross primary production (GPP). A large fraction of GPP realized each day is respired at night by plant maintenance respiration. The seasonal trend of the nighttime misfit between CDS and SAC thus indicates that the model underestimates plant respiration at night, and thus possibly GPP in the day. Although it is impossible to negate other hypotheses related to the atmospheric transport and vertical mixing, this result suggests that modeling nighttime CO₂ at rural stations is affected by systematic errors of respiration during the growing season, so that nighttime rural CO₂ data can hardly be used in atmospheric inversions for inferring anthropogenic emissions.

Further insight on the CO₂ concentration dynamics at SAC is provided by the vertical differences that are derived from the measurements at two levels, 15 m and 100 m AGL, on a tall tower at that location (Figure 9). During the afternoon, the differences are small and there is little agreement between the observations and the simulated values (Figure 9a). This systematic bias between the observed and simulated CO₂ vertical gradients could be explained by an underestimation of the photosynthetic uptake. The vertical CO₂ differences are much larger at night with a fair agreement between the measurements and the simulated values in wintertime (Figure 9b). Although the nighttime time series show strong similarities, there is a significant bias between the observations and the model during the growing season, but not so during the non-growing season. The seasonal phase of the vertical misfit is well correlated with the one obtained from the horizontal diagnostics, which tends to indicate the same bias in the estimated nighttime respiration.

The analyses of both Figure 8 and 9, together with similar results observed at other stations (Figure S3: e.g. the horizontal difference between CDS and COU, and the vertical difference at TRN), are consistent with the hypothesis that the respiration emission at night is underestimated by the VPRM model. Since nighttime respiration is usually well correlated with daytime respiration



(Reichstein et al., 2005), this result implies that the modeled positive gradients of CO₂ between urban and rural stations are probably overestimated during the growing season, so that without any optimization of respiration, an inversion would tend to generate a positive bias in the anthropogenic emissions estimates, to compensate for the negative bias in the respiration from VPRM.

3.2.3 Atmospheric transport

5 Uncertainty in simulated CO₂ due to transport errors can be evaluated empirically through the spread of simulated CO₂ by sensitivity experiments with different physical configurations of WRF-Chem. We have made five sensitivity simulations using the same surface fluxes and boundary conditions, but with three PBL schemes and two urban canopy schemes (see Table 1a).
10 Figure 10a shows the horizontal distribution of the monthly median standard deviation of simulated hourly CO₂ concentrations at approximately 20 m AGL using different physics schemes for two periods of the day (afternoon 11-16 UTC, nighttime 00-05 UTC), and for two months (January, July 2016). During January, the simulated CO₂ concentrations within the city, both in afternoon and nighttime, are highly sensitive to the choice of the physics scheme, with median standard deviations larger than 6 ppm. In contrast, the choice of the physics scheme has less influence on simulated CO₂ concentrations over suburban and rural areas in winter, with the median standard deviations of 1.2 ppm in the afternoon and 2 ppm at night. During the summer period, the smallest uncertainty of simulated CO₂ concentration resulting from different physics schemes is found in the afternoon with median standard deviations that are less than 1 ppm, which indicates that the various schemes provide very similar values. However, it is necessary to compare these standard deviations to the amplitudes of the anthropogenic emission signature. We thus calculated the median ratios of the simulated anthropogenic CO₂ concentration (average over the five sensitivity runs) to its respective standard deviation of the total CO₂ signals among the five sensitivity runs, which we define as the “signal-to-noise ratio” (Figure 10b). Indeed, the anthropogenic signal may be understood as the “signal” for the estimate of the emission, while the spread of the five sensitivity simulations provides an indicator of the atmospheric transport uncertainty. The largest signal-to-noise ratio is found in the afternoon of summer within the urban area, indicating that the link between the anthropogenic emission and the CO₂ concentration can be derived from the model with the highest confidence for these conditions. However, during the summer, the nighttime CO₂ measurements over the entire suburbs are poorly suited for the inversion since the simulated CO₂ are highly sensitive to the choice of physics scheme and the signal-to-noise ratios are then relatively small (< 1).
15 Figure 10c shows the vertical distribution along a south-north transect through the JUS station in a similar way as Figure 10a. In general, the simulations with various physics options show very large variations in the modeled CO₂ concentrations (up to 7.5 ppm standard deviation) close to the surface, a few tens of meters above the emissions. The differences become much smaller (less than 1 ppm) with increasing altitude. This may be due to the fact that different physics schemes lead to different vertical mixing efficiencies, which has a strong impact on the vertical structure of CO₂ concentrations. Given that the measurements are acquired at a level where the vertical gradient is large and variable, it may also indicate that the measurement-model discrepancy is highly dependent on the physics parameterization in the representation of the vertical mixing process in near-surface layers. During the winter period, there is a considerable difference in the vertical concentration profiles reproduced by different physics schemes within the city, with the uncertainty extending to a higher altitude in the afternoon than those in the nighttime. Further away from the urban area, anthropogenic emissions are substantially lower, and the vertical gradient of CO₂ generated by the strong city emission is smoothed out by the convection and diffusion processes. As a consequence, much less uncertainty is associated with the choice of the physics scheme in the suburbs at altitudes above ~200 m AGL. As for the signal-to-noise ratio shown in Figure 10d, the large values within the city tend to indicate that the urban CO₂ data are well suited for an estimate of the emissions using the atmospheric inversion method.
20
25
30
35



We also accessed the respective contributions of anthropogenic and biogenic fluxes to the simulated spread of CO₂ concentrations using different physics schemes. This allows us to provide a characterization of the impact of uncertainties in the atmospheric transport modeling along with that of the impact of the individual fluxes. Figure 11 shows the simulated monthly mean plus/minus one standard deviation of both the anthropogenic and biogenic CO₂ differences at approximately 20 m AGL between the control run (BEP_MYJ) and each of the other four sensitivity runs. The results in this figure are presented with the consideration of (i) two periods of the day (afternoon 11-16 UTC, nighttime 00-05 UTC); (ii) two months (January, July 2016); and (iii) three land use types (urban, crop and the others). Urban (7.4%) and crop (84.6%) are the two dominant land use types of the innermost model domain (D03) from the MODIS land cover database used in the WRF-Chem model, where the percentages in parenthesis indicate the proportion of each land use category to the total area. The other land use types (8.0%) mainly include grass, shrub, mixed forest, deciduous forest and evergreen forest. During the winter, the simulated anthropogenic CO₂ concentrations over the urban area are sensitive to the choice of the urban canopy scheme used in WRF-Chem, which is characterized by a substantial decrease in standard deviation from UCM to BEP (Figure 11a). The three simulations using the UCM scheme tend to produce higher anthropogenic CO₂ concentrations together with larger standard deviations with respect to the control run using the BEP scheme. On the other hand, these two urban canopy schemes (UCM, BEP) show small spreads in the simulation of anthropogenic CO₂ concentrations over the rural vegetated area for both seasons. This indicates that the choice of an urban canopy scheme is critical for simulating atmospheric transport at urban stations, but that the transport errors, without such scheme, remain mainly ‘local’ and have little remote influence at rural sites. That is, the choice of an urban scheme impacts CO₂ concentrations over the urban areas but its impact on the larger scale transport is not significant enough to affect the simulated concentrations over rural areas. During the summer period, our results show that the modeled nighttime CO₂ concentrations are strongly sensitive to both the urban canopy and PBL schemes. This conclusion applies to both the urban and the rural areas. Interestingly, the control run simulates higher nighttime CO₂ concentrations than the other four experiments.

Here, we quantify the uncertainty in the modeling results that is linked to the three PBL schemes and two urban canopy schemes. Clearly, there are other potential sources of atmospheric transport uncertainties that are not accounted for in this study. The simulated CO₂ differences among the ensemble of physics schemes tested here are therefore only a fraction of the full magnitude of model uncertainty. Nevertheless, this uncertainty is, in some cases, of similar magnitude as the measurement-model differences that have been shown in section 3.1.

3.2.4 Boundary condition

To investigate the uncertainty in CO₂ boundary conditions, we examined the modeled CO₂ sensitivity over the Paris region to the use of two different global CO₂ atmospheric inversion products as initial and boundary conditions for WRF-Chem (see Table 1c). Figure 12 shows all hourly CO₂ concentration differences between BEP_MYJ and BEP_MYJ_CT that used CO₂ fields from CAMS and CarbonTracker products respectively. The comparison is based on the simulated CO₂ in the 25-km grid cell of the outermost domain (D01) containing the Paris city. For most time of the year (~73%), the differences in simulated CO₂ concentrations over Paris are within the range of ±1 ppm since they are mainly affected by those differences between CAMS and CarbonTracker at the western boundary of D01 under the influence of west winds. Nevertheless, considerable differences (up to 5 ppm) are observed during several synoptic episodes, which illustrates the magnitude of uncertainties linked with the boundary condition hypothesis. These magnitudes are similar to those of the impacts of different physics schemes on simulated CO₂ concentrations over suburban and rural areas as shown in section 3.2.3. Under such circumstances, it requires the use of additional observations to constrain the boundary inflow in inversions. On the other hand, as the IdF region is exposed to a relatively well-mixed background atmosphere after a long-range transport of CO₂ from remote sources and sinks, one may expect that the resulting CO₂ concentration features



are large scales. As a consequence, the potential modeling error induced by an erroneous boundary will be similar for monitoring stations located within Paris and its vicinity. This characteristic suggests that the assimilation of upwind-downwind gradient in CO₂ concentrations in the inversion of city-scale emissions as done in previous studies could also be an effective way to minimize the potential biases both from the boundary conditions and from remote fluxes within the domain but outside the city (Bréon et al., 2015; Stauffer et al., 2016).

4 Conclusions and discussions

We have analyzed CO₂ concentrations measured and modeled at six stations located within and in the surrounding of the Paris city. Our objective is to identify the main causes of the CO₂ differences between the measurements and their simulated counterparts, with the overall goal to improve the quantification of anthropogenic emissions. To accomplish this, we have performed an ensemble-based sensitivity study and a full analysis of the uncertainties linked to anthropogenic inventories, biogenic fluxes, atmospheric transports and boundary conditions, either focusing on limited periods or looking at the full-year period.

A preliminary identification of the modeling errors was first conducted with the KNN algorithm to identify the largest mismatches between the observations and the model results. These large discrepancies are either related to specific measurement contaminations from local unresolved sources of CO₂ emissions, or to the model's inability to properly simulate the atmospheric transport for specific meteorological conditions. It is therefore necessary to explicitly discard these outliers for any atmospheric inversion that aims at the city emissions.

Within the city, the modeled CO₂ concentrations appear highly sensitive not only to the atmospheric vertical mixing close to the surface, but also to the prescribed temporal profile of anthropogenic emissions. These sources of errors are large, particularly in winter, and show a potential for biases that is problematic when aiming at quantification of city emissions. There is little hope to significantly decrease these uncertainty factors in the near future, unless better constraints on transport such as vertical profiles, could be available. Such complementary measurements will be of great help to understand the characteristics of CO₂ vertical distribution under both stable and convective boundary-layer conditions. It can also be used to verify and validate the atmospheric transport model, and to reduce transport errors based on the data assimilation technique.

In the suburbs, further away from the urban sources, the anthropogenic emissions are lower and the vertical gradient of CO₂ concentration, generated by the city emissions, is smoothed out by the atmospheric convection and diffusion processes. There is then less uncertainty than within the city about the efficiency of the vertical mixing. The link between the anthropogenic emission and the CO₂ concentration during the afternoon in winter can then be derived from the model with more confidence. However, the contribution of the biogenic flux to the CO₂ concentration is an issue during the growing season. The difficulty is mainly related to the simulation of the nocturnal CO₂ concentrations because of the large uncertainties in the atmospheric transport modeling as well as the biogenic fluxes. Additional measurements of carbon isotopes (¹⁴C, ¹³C) and tracers coemitted with CO₂ (e.g., CO, NO_x) could be used to separate the contributions from fossil fuel and biogenic components to the total CO₂ concentrations, which would be beneficial for the optimization of sectoral CO₂ fluxes.

The influence of different CO₂ boundary conditions for our model domain is dependent on synoptic weather situations. As for the Paris region, the simulated CO₂ differences between CAMS and CarbonTracker are less than one ppm during most periods of westerly winds that bring in clean oceanic air masses, but they can vary by several ppm during some synoptic episodes, e.g. with north and easterly winds. This result advocates the practice of using additional observations to constrain the boundary inflow, or using CO₂ gradients when the wind direction is properly aligned with two (upwind-downwind) stations in the inversion of CO₂ fluxes of the Paris region.



Our analyses confirm the difficulty of accurately modeling the atmospheric CO₂ concentration within and in the close vicinity of urban areas. Although we have pointed out the likely causes for the measurement-model discrepancies, we have not been able to unambiguously demonstrate the respective contributions of anthropogenic emissions, biogenic fluxes and atmospheric transport errors. This is a strong cause of concern for the objective of measuring the city emissions on the basis of atmospheric concentrations.

5 It has been argued that, rather than measuring the absolute emission, the atmospheric inversion approach should aim at the emissions changes, with the argument that atmospheric transport biases would not change, and thus let any emission variation show up in the concentrations. However, one may argue that a significant change in the total emission would be associated with a change in its spatial distribution and/or a change in the temporal profile. These would then also impact the relationship between the emission and the concentration.

10 **Author contribution**

JL, FMB, GB and PC contributed to the design and implementation of the research. JL, FMB, GB, BZ and PC contributed to the analysis and interpretation of the results. MR performed the measurements. JL and FMB took the lead in writing the manuscript with input from all authors.

Code/Data availability

15 All data sets and model results corresponding to this study are available upon request from the corresponding author.

Competing interests

The authors have no competing interests to declare.

Acknowledgements

20 This work is supported by the Ph.D. program funded by the IDEX Paris-Saclay, ANR-11-IDEX-0003-02 together with Harris Corporation. We would like to thank Harris Corporation for the support of these ongoing analyses. Thanks also to Marc Jamous at Cité des Sciences et de l'Industrie (CDS), to Cristelle Cailteau-Fischbach (LATMOS/IPSL), to OVSQ, and to LSCE/RAMCES technical staff for the maintenance of the in-situ monitoring network, coordinated by Delphine Combaz.

References

- 25 Ahmadov, R., Gerbig, C., Kretschmer, R., Koerner, S., Neininger, B., Dolman, A. J., and Sarrat, C.: Mesoscale covariance of transport and CO₂ fluxes: Evidence from observations and simulations using the WRF-VPRM coupled atmosphere-biosphere model. *Journal of Geophysical Research: Atmospheres*, 112(D22), 2007.
- Ahmadov, R., Gerbig, C., Kretschmer, R., Körner, S., Rördenbeck, C., Bousquet, P., and Ramonet, M.: Comparing high resolution WRF-VPRM simulations and two global CO₂ transport models with coastal tower measurements of CO₂. *Biogeosciences*, 6(5): 807-817, 2009.
- 30 AIRPARIF: Bilan des émissions de polluants atmosphériques et de gaz à effet de serre en Île-de-France pour l'année 2010 et historique 2000/2005, available at: https://www.airparif.asso.fr/_pdf/publications/Emissions_2010_CG75.pdf (last access: 20 April 2019), 2013.
- Berrisford, P., Dee, D., Poli, P., Brugge, R., Fielding, K., Fuentes, M., Kallberg, P., Kobayashi, S., Uppala, S., and Simmons, A.: The ERA-Interim archive, version 2.0, 2011.



- Boon, A., Broquet, G., Clifford, D. J., Chevallier, F., Butterfield, D. M., Pison, I., Ramonet, M., Paris, J. D. and Ciais, P.: Analysis of the potential of near-ground measurements of CO₂ and CH₄ in London, UK, for the monitoring of city-scale emissions using an atmospheric transport model. *Atmospheric Chemistry and Physics*, 16(11): 6735-6756, 2016.
- 5 Bougeault, P., and Lacarrere, P.: Parameterization of orography-induced turbulence in a mesobeta-scale model. *Monthly Weather Review*, 117(8), 1872-1890, 1989.
- Brón, F. M., Broquet, G., Puygrenier, V., Chevallier, F., Xueref-Remy, I., Ramonet, M., Dieudonné E., Lopez, M., Schmidt, M., Perrussel, O., and Ciais, P.: An attempt at estimating Paris area CO₂ emissions from atmospheric concentration measurements. *Atmospheric Chemistry and Physics*, 15(4): 1707-1724, 2015.
- 10 Broquet, G., Brón, F. M., Renault, E., Buchwitz, M., Reuter, M., Bovensmann, H., Chevallier, F., Wu, L., and Ciais, P.: The potential of satellite spectro-imagery for monitoring CO₂ emissions from large cities, *Atmospheric Measurement Techniques*, 11, 681-708, 2018.
- Bulletin Climatique Météo-France, 2016.
https://donneespubliques.meteofrance.fr/?fond=produit&id_produit=129&id_rubrique=29 (last access: 1 October 2019)
- 15 Chen, F., and Dudhia, J.: Coupling an advanced land surface-hydrology model with the Penn State-NCAR MM5 modeling system. Part I: Model implementation and sensitivity. *Monthly Weather Review*, 129(4): 569-585, 2001.
- Chen, F., Kusaka, H., Bornstein, R., Ching, J., Grimmond, C. S. B., Grossman-Clarke, S., Loridan, T., Manning, K. W., Martilli, A., Miao, S., Sailor, D., Salamanca, F. P., Taha, H., Tewari, M., Wang, X., Wyszogrodzki, A. A., and Zhang, C.: The integrated WRF/urban modelling system: development, evaluation, and applications to urban environmental problems. *International Journal of Climatology*, 31(2): 273-288, 2011.
- 20 Chevallier, F.: Description of the CO₂ inversion production chain. CAMS deliverable CAMS73_2015SC2_D73.1.5.5_201703_CO₂ inversion production chain_v1. <http://atmosphere.copernicus.eu/>, 2017a.
- Chevallier, F.: Validation report for the inverted CO₂ fluxes, v1r1. CAMS deliverable CAMS73_2015SC2_D73.1.4.2-1979-2016-v1_201707. <http://atmosphere.copernicus.eu/>, 2017b.
- 25 Deng, A., Lauvaux, T., Davis, K.J., Gaudet, B.J., Miles, N., Richardson, S.J., Wu, K., Sarmiento, D.P., Hardesty, R.M., Bonin, T.A., Brewer, W.A. and Gurney, K.R.: Toward reduced transport errors in a high resolution urban CO₂ inversion system. *Elem Sci Anth*, 5, p.20, 2017.
- Dudhia, J.: Numerical study of convection observed during the winter monsoon experiment using a mesoscale two-dimensional model. *Journal of the Atmospheric Sciences*, 46(20): 3077-3107, 1989.
- 30 Dupont E, Menut L, Carissimo B, et al. Comparison between the atmospheric boundary layer in Paris and its rural suburbs during the ECLAP experiment. *Atmospheric Environment*, 33(6): 979-994, 1999.
- Feng, S., Lauvaux, T., Newman, S., Rao, P., Ahmadov, R., Deng, A., Díaz-Isaac, L. I., Duren, R. M., Fischer, M. L., Gerbig, C., Gurney, K. R., Huang, J., Jeong, S., Li, Z., Miller, C. E., O’Keefe, D., Patarasuk, R., Sander, S. P., Song, Y., Wong, K. W., and Yung, Y. L.: Los Angeles megacity: a high-resolution land-atmosphere modelling system for urban CO₂ emissions. *Atmospheric Chemistry and Physics*, 16(14): 9019-9045, 2016.
- 35 Gately, C. K., and Hutrya, L. R.: Large uncertainties in urban-scale carbon emissions. *Journal of Geophysical Research: Atmospheres*, 122(20), 11-242, 2017.
- Göckede, M., Turner, D. P., Michalak, A. M., Vickers, D., and Law, B. E.: Sensitivity of a subregional scale atmospheric inverse CO₂ modeling framework to boundary conditions. *Journal of Geophysical Research: Atmospheres*, 115(D24), 2010.
- 40 Grell, G. A., and Dévényi, D.: A generalized approach to parameterizing convection combining ensemble and data assimilation techniques. *Geophysical Research Letters*, 29(14): 38-1-38-4, 2002.
- Grell, G. A., Peckham, S. E., Schmitz, R., McKeen, S. A., Frost, G., Skamarock, W. C., and Eder, B.: Fully coupled “online” chemistry within the WRF model. *Atmospheric Environment*, 39, 6957-6975, 2005.
- Hardiman, B. S., Wang, J. A., Hutrya, L. R., Gately, C. K., Getson, J. M., and Friedl, M. A.: Accounting for urban biogenic fluxes in regional carbon budgets. *Science of the Total Environment*, 592, 366-372, 2017.
- 45 Hong, S. Y., and Lim, J. O. J.: The WRF single-moment 6-class microphysics scheme (WSM6). *Journal of the Korean Meteorological Society*, 42(2): 129-151, 2006.
- Hong, S. Y., Noh, Y., and Dudhia, J.: A new vertical diffusion package with an explicit treatment of entrainment processes. *Monthly Weather Review*, 134(9): 2318-2341, 2006.
- IEA: World energy outlook, International Energy Agency (IEA), 2016.



- Janjić, Z. I.: The step-mountain coordinate: Physical package. *Monthly Weather Review*, 118(7), 1429-1443, 1990.
- Janjić, Z. I.: The step-mountain eta coordinate model: Further developments of the convection, viscous sublayer, and turbulence closure schemes. *Monthly Weather Review*, 122(5): 927-945, 1994.
- Janjić, Z.I.: The surface layer in the NCEP Eta Model. Eleventh Conference on Numerical Weather Prediction, Norfolk, VA, 19-23 August 1996. American Meteorological Society, Boston, MA, 354-355, 1996.
- 5 Jiméñez, P. A., and Dudhia, J.: Improving the representation of resolved and unresolved topographic effects on surface wind in the WRF model. *Journal of Applied Meteorology and Climatology*, 51(2): 300-316, 2012.
- Lauvaux, T., Schuh, A. E., Uliasz, M., Richardson, S., Miles, N., Andrews, A. E., Sweeney, C., Diaz, L. I., Martins, D., Shepson, P. B., and Davis, K. J.: Constraining the CO₂ budget of the corn belt: exploring uncertainties from the assumptions in a mesoscale inverse system, *Atmospheric Chemistry and Physics*, 12, 337-354, 2012.
- 10 Lauvaux, T., Miles, N. L., Deng, A., Richardson, S. J., Cambaliza, M. O., Davis, K. J., Gaudet, B., Gurney, K. R., Huang, J., O’Keeffe, D., Song, Y., Karion, A., Oda, T., Patarasuk, R., Sarmiento, D., Shepson, P., Sweeney, C., Turnbull, J., and Wu, K.: High-resolution atmospheric inversion of urban CO₂ emissions during the dormant season of the Indianapolis Flux Experiment (INFLUX). *Journal of Geophysical Research: Atmospheres*, 121(10): 5213-5236, 2016.
- 15 Le Quéré C., Andrew, R. M., Friedlingstein, P., Sitch, S., Hauck, J., Pongratz, J., Pickers, P. A., Korsbakken, J. I., Peters, G. P., Canadell, J. G., Arneeth, A., Arora, V. K., Barbero, L., Bastos, A., Bopp, L., Chevallier, F., Chini, L. P., Ciais, P., Doney, S. C., Gkritzalis, T., Goll, D. S., Harris, I., Haverd, V., Hoffman, F. M., Hoppema, M., Houghton, R. A., Hurtt, G., Ilyina, T., Jain, A. K., Johannessen, T., Jones, C. D., Kato, E., Keeling, R. F., Goldewijk, K. K., Landschützer, P., Lefèvre, N., Lienert, S., Liu, Z., Lombardozi, D., Metz, N., Munro, D. R., Nabel, J. E. M. S., Nakaoka, S., Neill, C., Olsen, A., Ono, T., Patra, P., Peregon, A., Peters, W., Peylin, P., Pfeil, B., Pierrot, D., Poulter, B., Rehder, G., Resplandy, L., Robertson, E., Rocher, M., Rödenbeck, C., Schuster, U., Schwinger, J., Sérian, R., Skjelvan, I., Steinhoff, T., Sutton, A., Tans, P. P., Tian, H., Tilbrook, B., Tubiello, F. N., van der Laan-Luijkx, I. T., van der Werf, G. R., Viovy, N., Walker, A. P., Wiltshire, A. J., Wright, R., Zaehle, S., and Zheng, B.: Global Carbon Budget 2018, *Earth System Science Data*, 10, 2141-2194, 2018.
- 20 Lian, J., Wu, L., Brón, F. M., Broquet, G., Vautard, R., Zaccheo, T. S., Dobler, J., and Ciais, P.: Evaluation of the WRF-UCM mesoscale model and ECMWF global operational forecasts over the Paris region in the prospect of tracer atmospheric transport modeling. *Elem Sci Anth*, 6:64, 2018.
- Lian, J., Brón, F. M., Broquet, G., Zaccheo, T. S., Dobler, J., Ramonet, M., Staufer, J., Santaren, D., Xueref-Remy, I., and Ciais, P.: Analysis of temporal and spatial variability of atmospheric CO₂ concentration within Paris from the GreenLITE™ laser imaging experiment. *Atmospheric Chemistry and Physics*, 19, 13809-13825, 2019.
- 30 Mahadevan, P., Wofsy, S. C., Matross, D. M., Xiao, X., Dunn, A. L., Lin, J. C., Gerbig, C., Munger, J. W., Chow, V. Y., and Gottlieb, E. W.: A satellite-based biosphere parameterization for net ecosystem CO₂ exchange: Vegetation Photosynthesis and Respiration Model (VPRM). *Global Biogeochemical Cycles*, 22(2), 2008.
- Martilli, A., Clappier, A., and Rotach, M. W.: An urban surface exchange parameterisation for mesoscale models. *Boundary-Layer Meteorology*, 104(2), 261-304, 2002.
- 35 Martin, C. R., Zeng, N., Karion, A., Mueller, K., Ghosh, S., Lopez-Coto, I., Gurney, K. R., Oda, T., Prasad, K., Liu, Y., Dickerson, R. R., and Whetstone, J.: Investigating sources of variability and error in simulations of carbon dioxide in an urban region. *Atmospheric Environment*, 199, 55-69, 2019.
- Mlawer, E. J., Taubman, S. J., Brown, P. D., Iacono, M. J., and Clough, S. A.: Radiative transfer for inhomogeneous atmospheres: RRTM, a validated correlated-k model for the longwave. *Journal of Geophysical Research: Atmospheres*, 102(D14): 16663-16682, 1997.
- 40 Nielsen-Gammon J. W., Powell, C. L., Mahoney, M. J., Angevine, W. M., Senff, C. J., White, A., Berkowitz, C., Doran, C., and Knupp, K.: Multisensor estimation of mixing heights over a coastal city. *Journal of Applied Meteorology and Climatology*, 47(1): 27-43, 2008.
- Nehr Korn, T., Henderson, J., Leidner, M., Mountain, M., Eluszkiewicz, J., McKain, K., and Wofsy, S.: WRF simulations of the urban circulation in the Salt Lake City area for CO₂ modeling. *Journal of Applied Meteorology and Climatology*, 52(2): 323-340, 2013.
- 45 Peters, W., Jacobson, A. R., Sweeney, C., Andrews, A. E., Conway, T. J., Masarie, K., Miller, J. B., Bruhwiler, L. M. P., Petron, G., Hirsch, A. I., Worthy, D. E. J., van der Werf, G. R., Randerson, J. T., Wennberg, P. O., Krol, M. C., and Tans, P. P: An atmospheric perspective on North American carbon dioxide exchange: CarbonTracker. *Proceedings of the National Academy of Sciences*, 104(48), 18925-18930, 2007.
- 50 Ramaswamy, S., Rastogi, R., and Shim, K.: Efficient algorithms for mining outliers from large data sets. In *ACM Sigmod Record* (Vol. 29, No. 2, pp. 427-438). ACM, 2000.



- 5 Reichstein, M., Falge, E., Baldocchi, D., Papale, D., Aubinet, M., Berbigier, P., Bernhofer, C., Buchmann, N., Gilmanov, T., Granier, A., Grunwald, T., Havrankova, K., Ilvesniemi, H., Janous, D., Knohl, A., Laurila, T., Lohila, A., Loustau, D., Matteucci, G., Meyers, T., Miglietta, F., Ourcival, J. M., Pumpanen, J., Rambal, S., Rotenberg, E., Sanz, M., Tenhunen, J., Seufert, G., Vaccari, F., Vesala, T., Yakir, D., Valentini, R.: On the separation of net ecosystem exchange into assimilation and ecosystem respiration: review and improved algorithm. *Global Change Biology*, 11(9), 1424-1439, 2005.
- Seto, K. C., Dhakal, S., Bigio, A., Blanco, H., Delgado, G. C., Dewar, D., Huang, L., Inaba, A., Kansal, A., Lwasa, S., McMahon, J., Müller, D. B., Murakami, J., Nagendra, H., and Ramaswami, A.: Human settlements, infrastructure and spatial planning, chap. 12, in: *Climate Change 2014: Mitigation of Climate Change. IPCC Working Group III Contribution to AR5*. Cambridge University Press, Cambridge, UK and New York, NY, USA, 2014.
- 10 Staufer, J., Broquet, G., Brón, F. M., Puygrenier, V., Chevallier, F., Xueref-Rény, I., Dieudonné E., Lopez, M., Schmidt, M., Ramonet, M., Perrussel, O., Lac, C., Wu, L., and Ciais, P.: The first 1-year-long estimate of the Paris region fossil fuel CO₂ emissions based on atmospheric inversion. *Atmospheric Chemistry and Physics*, 16(22): 14703-14726, 2016.
- Tans, P., Zhao, C., and Kitzis, D.: The WMO Mole Fraction Scales for CO₂ and other greenhouse gases, and uncertainty of the atmospheric measurements, Report of the 15th WMO/IAEA Meeting of Experts on Carbon Dioxide, Other Greenhouse Gases, and Related Measurement Techniques, 7-10 September 2009, GAW Report No. 194, WMO TD No. 1553, 152-159, 2011.
- 15 United Nations, Department of Economic and Social Affairs, Population Division. *World Population Prospects 2019: Highlights (ST/ESA/SER.A/423)*, available at: https://population.un.org/wpp/Publications/Files/WPP2019_Highlights.pdf (last access: November, 2019), 2019.
- 20 Wu, L., Broquet, G., Ciais, P., Bellassen, V., Vogel, F., Chevallier, F., Xueref-Remy, I., and Wang, Y.: What would dense atmospheric observation networks bring to the quantification of city CO₂ emissions?, *Atmospheric Chemistry and Physics*, 16(12): 7743-7771, 2016.
- Xueref-Remy, I., Dieudonné E., Vuillemin, C., Lopez, M., Lac, C., Schmidt, M., Delmotte, M., Chevallier, F., Ravetta, F., Perrussel, O., Ciais, P., Brón, F. M., Broquet, G., Ramonet, M., Spain, T. G., and Ampe, C.: Diurnal, synoptic and seasonal variability of atmospheric CO₂ in the Paris megacity area. *Atmospheric Chemistry and Physics*, 18, 3335-3362, 2018.
- 25 Zhao, Y., Nasrullah, Z., and Li, Z.: PyOD: A python toolbox for scalable outlier detection. *Journal of Machine Learning Research*, 20(96), 1-7, 2019.

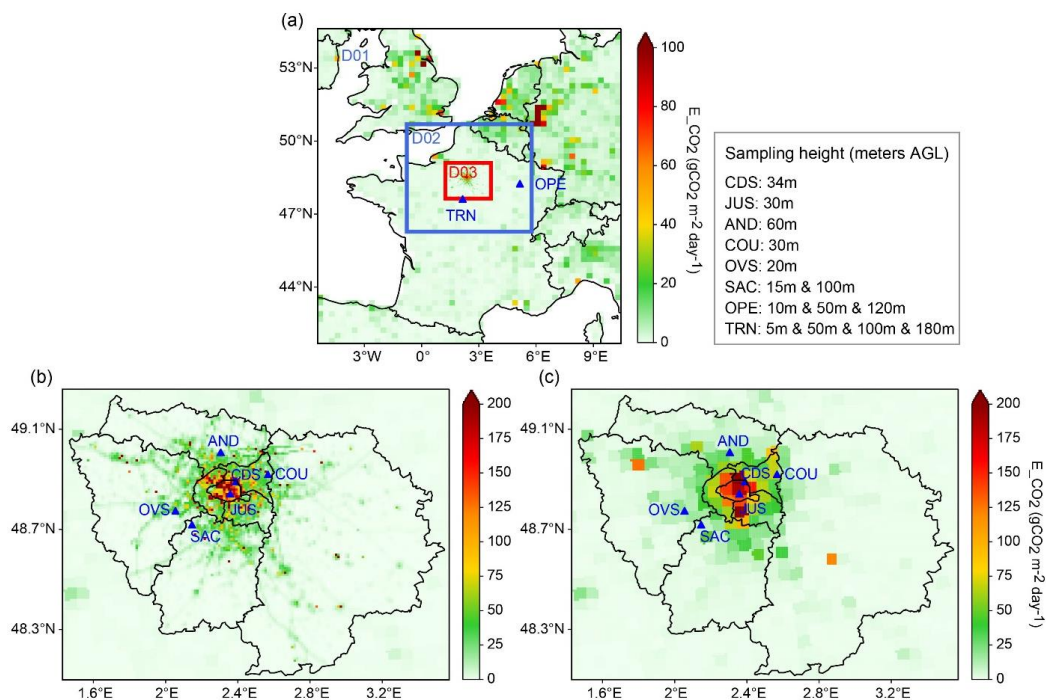


Figure 1: (a) Three domains of WRF-Chem that are used for the simulations discussed in this study, together with the large-scale CO₂ emission for a weekday in November; Distributions of CO₂ emissions for a typical weekday in November from the (b) AirParif and (c) IER inventories. The bottom two maps show the location of six CO₂ measurement stations as well as the administrative limits of the Île-de-France region.

5

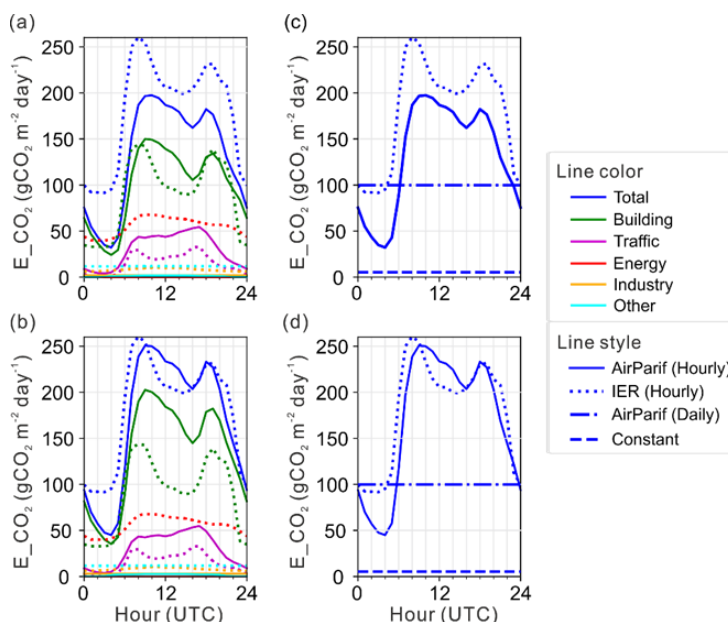


Figure 2: Diurnal profiles (for January) of anthropogenic emissions in the grid cell of the emission map containing the CDS station. (a) and (c) are for the 1-km grid cell of the AirParif emission inventory that contains the station, whereas (b) and (d) are the 5-km grid cell of the IER inventory around the same station. (a) and (b) show the emission by sectors, whereas (c) and (d) are for the total emissions together with the constant emission profiles as discussed in the text.

10

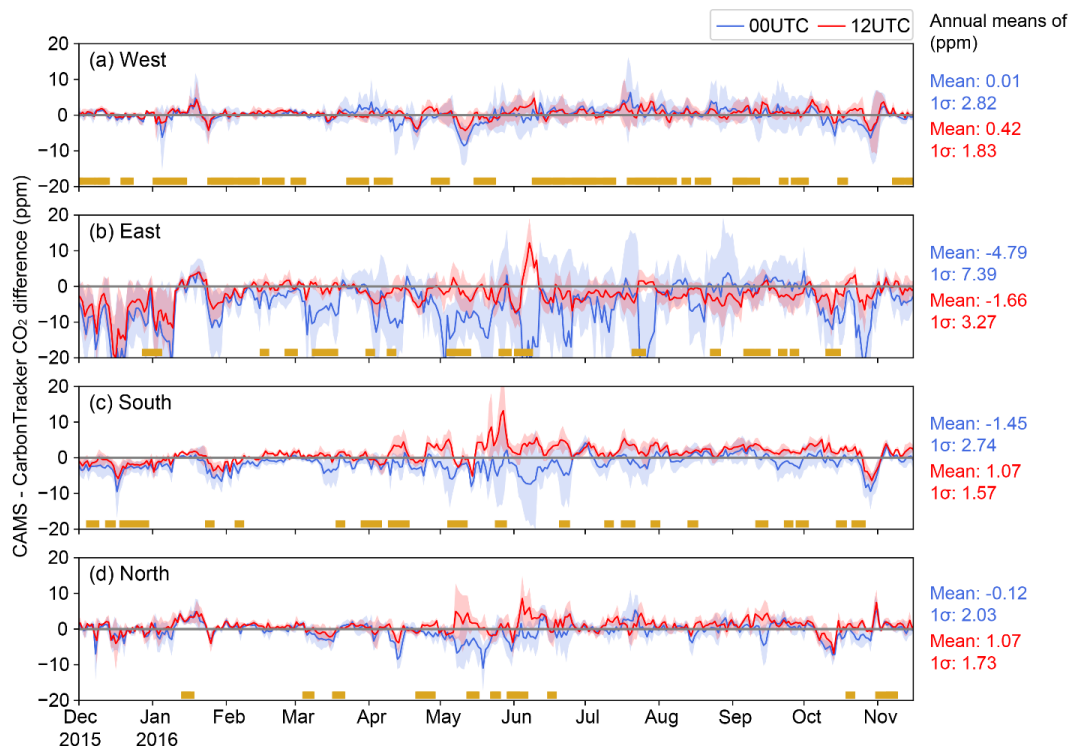


Figure 3: Time series of average CO₂ concentration differences between CAMS and CarbonTracker at four lateral boundaries (west, east, south, north), averaged over the lowest 0.7 km AGL, of D01 for 00 UTC in blue and 12 UTC in red. The lines indicate the spatial means over each boundary (a latitudinal transect for western and eastern boundaries / a longitudinal transect for southern and northern boundaries). The shaded areas extend over one standard deviation ($\pm 1\sigma$) computed over the grid cells that make the lateral boundary (spatial standard deviation). The yellow symbols indicate the days when the wind blows from outside of the domain at the respective domain boundary. The numbers on the right side of figure indicate annual means of (i) the spatial mean and (ii) the spatial standard deviation.

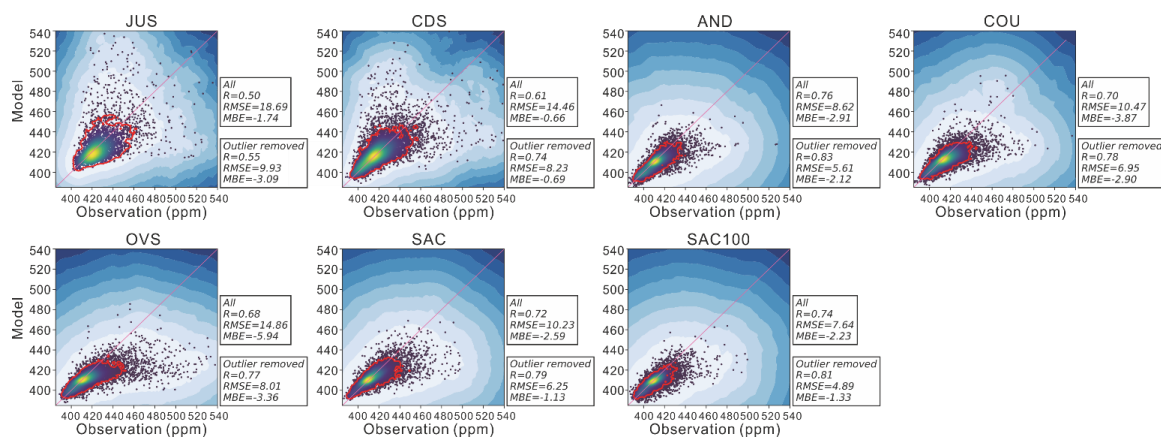
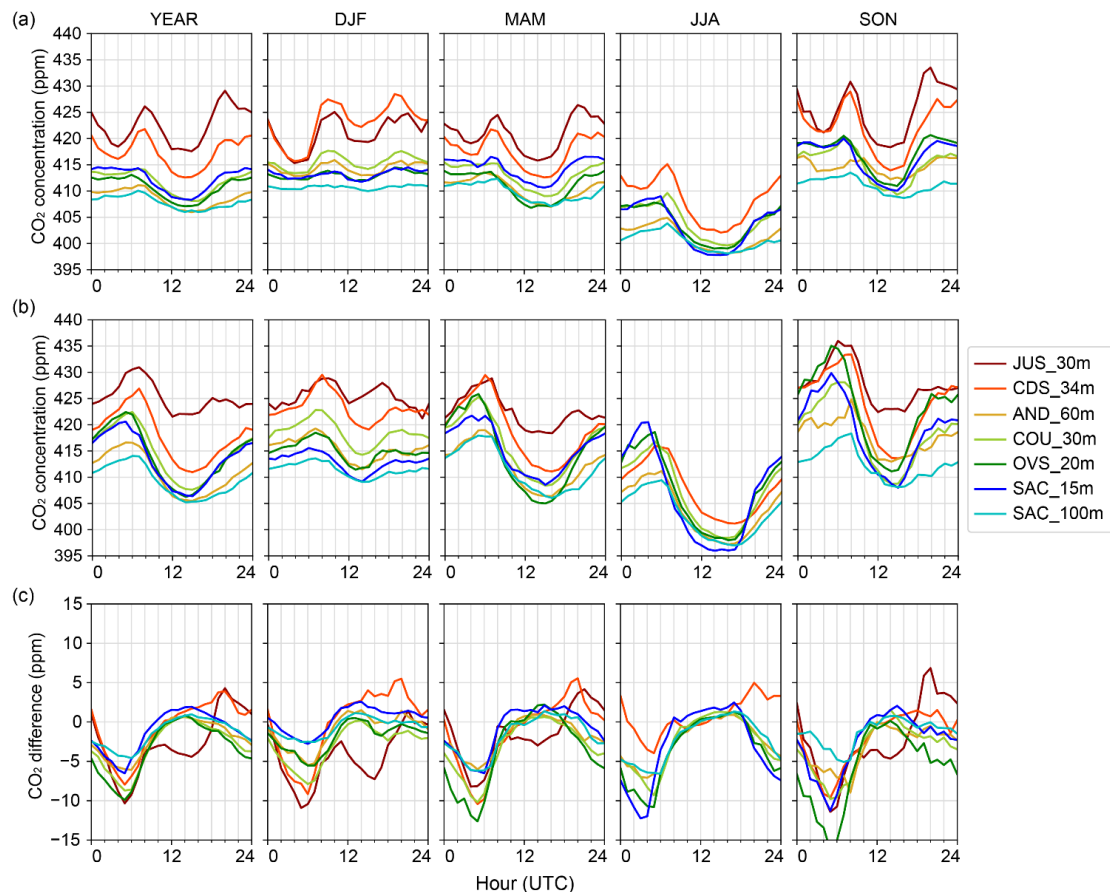
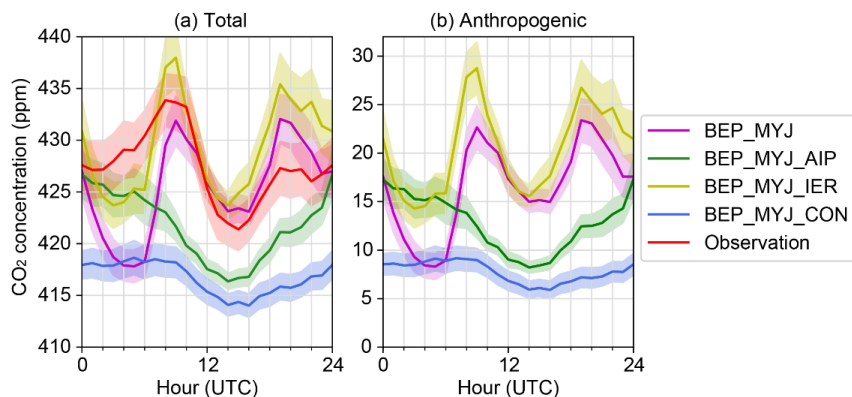


Figure 4: Observed and BEP_MYJ (control run) simulated all hourly CO₂ concentrations at six monitoring sites from December 2015 to November 2016. The color of dots represents the density of points at a given position. The shade of blue area indicates the anomaly score for each point, with the minimum in light blue and the threshold value in dark blue. The dots lying outside the red contour (threshold value) are the large model-observation misfits (outliers) detected by the K-nearest neighbors (KNN) algorithm with an outlier fraction of 0.1.



5 **Figure 5: Comparison of average diurnal variations between the (a) BEP_MYJ simulated (control run), (b) observed CO₂ concentrations, and (c) CO₂ differences between the model and the observations for four seasons. DJF denotes December-January-February, MAM denotes March-April-May, JJA denotes June-July-August and SON denotes September-October-November. The JUS instrument was not working during the summer of 2016.**



10 **Figure 6: Average diurnal cycle of (a) total and (b) anthropogenic CO₂ concentrations for the four experiments at CDS station. The shaded areas extend over the standard deviation of the CO₂ concentration divided by the square root of the number of observations.**

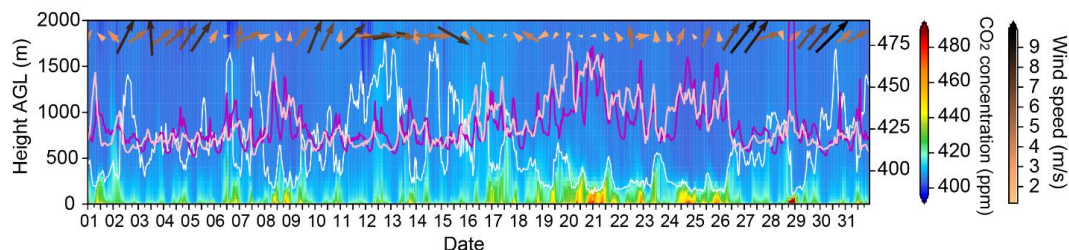


Figure 7: Vertical distribution of CO₂ concentrations at CDS station for January 2016, together with time series of BEP_MYJ simulated PBL heights in white, simulated CO₂ concentration in magenta and observed CO₂ concentration in pink. The simulation uses the AirParif CO₂ emission inventory. The arrows on the top of the figure indicate the wind speed and direction every day at noon and midnight.

5

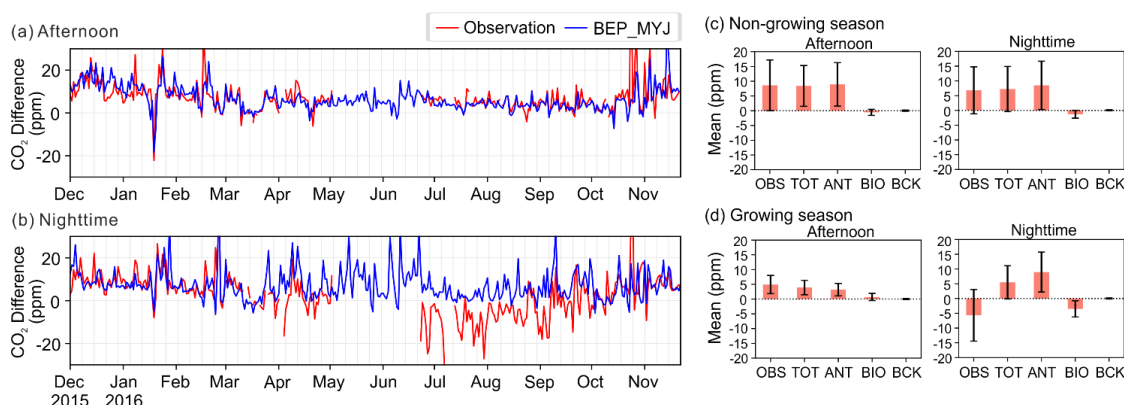


Figure 8: Daily (a) afternoon mean (11-16 UTC) and (b) nighttime mean (21-05 UTC) CO₂ horizontal differences between CDS and SAC. Daily CO₂ horizontal differences between CDS and SAC from each sector for (c) Non-growing season from October to April and (d) Growing season from May to September. OBS indicates the observed CO₂ concentration differences. TOT, ANT, BIO and BCK indicates the simulated total, anthropogenic, biogenic and background CO₂ concentration differences respectively.

10

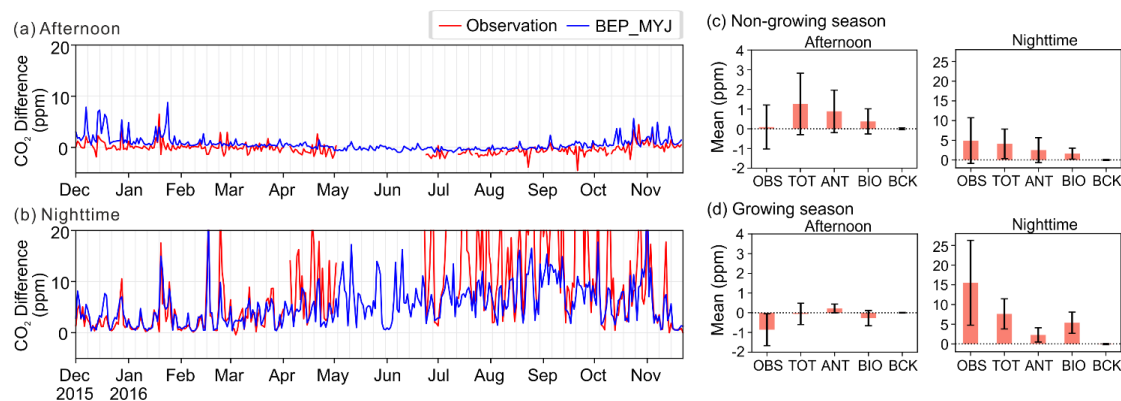


Figure 9: Daily (a) afternoon mean (11-16 UTC) and (b) nighttime mean (21-05 UTC) CO₂ vertical differences at SAC (15m-100m). Daily CO₂ vertical differences at SAC (15m-100m) from each sector for (c) Non-growing season from October to April and (d) Growing season from May to September. OBS indicates the observed CO₂ concentration differences. TOT, ANT, BIO and BCK indicates the simulated total, anthropogenic, biogenic and background CO₂ concentration differences respectively.

15

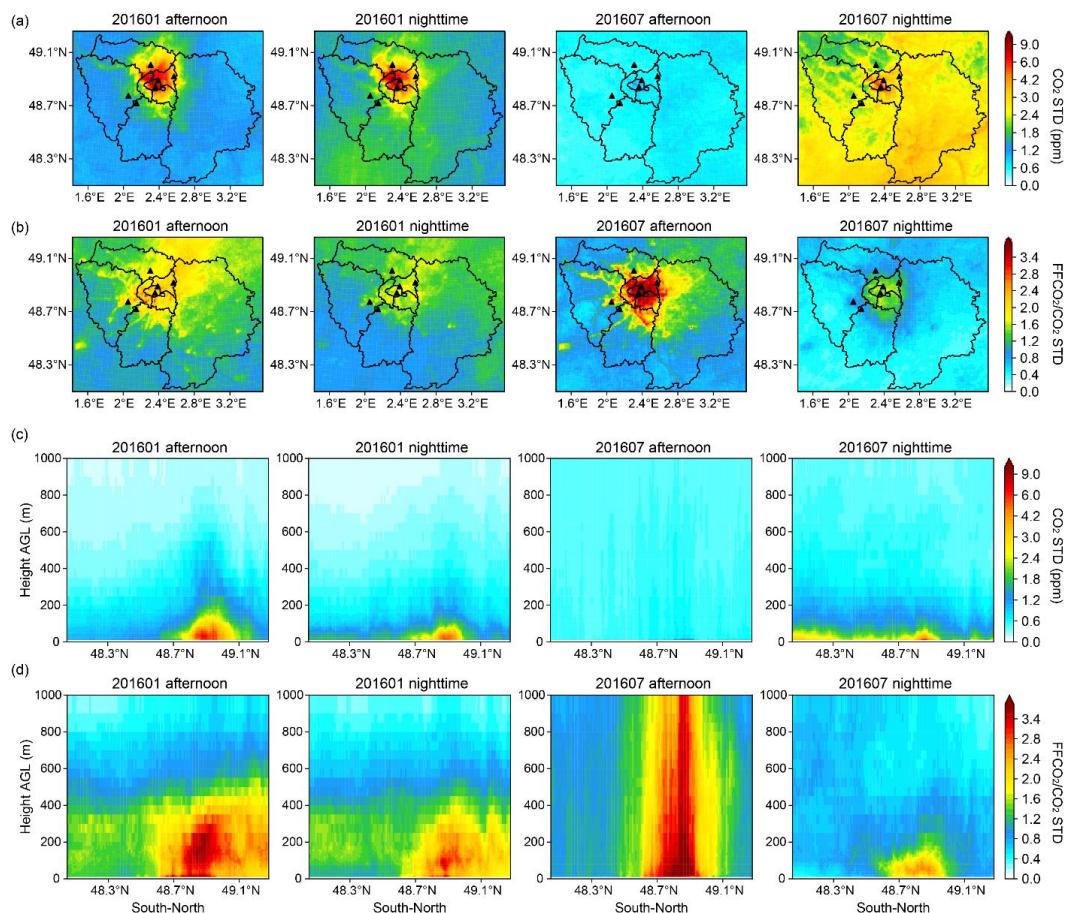


Figure 10: Analysis of the “signal-to-noise” as discussed in the text for two periods of the day (afternoon 11-16 UTC, nighttime 00-05 UTC), and two months (January, July 2016). (a) is the median of the hourly standard deviation of the simulated near-surface CO₂ concentration computed among the five sensitivity runs (Table 1a); (c) is the same as (a) but for a vertical south-north slice that goes through the JUS station; (b) is the median ratios of the hourly anthropogenic CO₂ concentration (average of the five sensitivity runs) to its respective standard deviation of the total CO₂ concentrations among the five sensitivity runs; (d) is the same as (b) but for the same vertical slice as in (c).

5

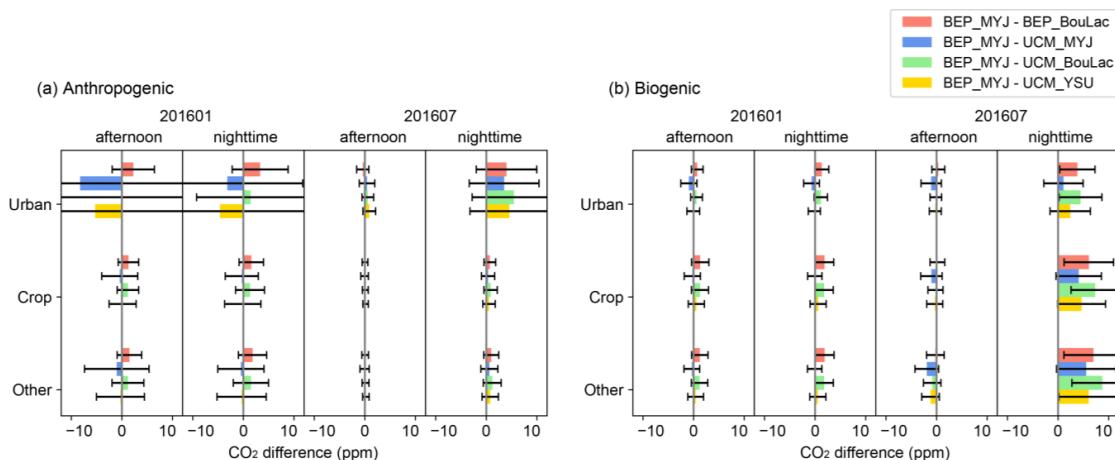


Figure 11. The simulated monthly mean plus/minus one standard deviation of the (a) anthropogenic and (b) biogenic CO₂ difference between the control run (BEP_MYJ) and the other four sensitivity runs for three land use types (urban, crop and the others), two periods of the day (afternoon 11-16 UTC, nighttime 00-05 UTC) and two months (January, July 2016).

5

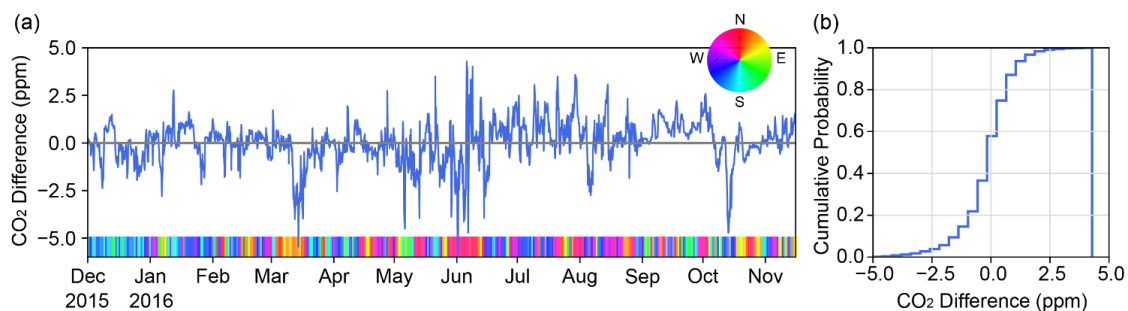


Figure 12. (a) Time series and (b) cumulative distribution of all hourly CO₂ concentration differences between BEP_MYJ and BEP_MYJ_CT using CAMS and CarbonTracker as CO₂ boundary conditions respectively. This comparison is based on the simulated values in the 25-km grid cell of the outermost domain (D01) containing the Paris city.

10

15



Table 1. Summary of WRF-Chem configurations used for the sensitivity experiments in this study. The bold text indicates the settings of the control run which is the same in all sets of sensitivity experiments.

(a) Sensitivity experiments of physics schemes carried out for a full-year period (2015.09-2016.11)

Configuration	PBL Scheme	Urban Canopy Scheme	Vertical Resolution	Anthropogenic Inventory	Boundary Condition
BEP_MYJ	MYJ	BEP	44 levels (wherein 25 below 1.5 km). The lowest layer top is around 3.8 m AGL	IER (5 km, outside IdF) + AirParif (1 km, within IdF) with hourly profile	CAMS
BEP_BouLac	BouLac				
UCM_MYJ	MYJ	UCM	34 levels (wherein 15 below 1.5 km). The lowest layer top is around 19 m AGL		
UCM_BouLac	BouLac				
UCM_YSU	YSU				

(b) Sensitivity experiments of anthropogenic emissions carried out for a one-month period (2016.01)

Configuration	Anthropogenic Inventory		PBL Scheme + Urban Canopy Scheme	Boundary Condition
BEP_MYJ	IER (5 km, outside IdF) + AirParif (1 km, within IdF)	with hourly profile	MYJ + BEP	CAMS
BEP_MYJ_AIP		without hourly profile		
BEP_MYJ_IER	IER (5 km)	with hourly profile		
BEP_MYJ_CON	Constant (5.28 gCO ₂ /m ² /day)			

5 (c) Sensitivity experiments of CO₂ boundary conditions carried out for the outermost domain (D01) for a full-year period (2015.09-2016.11)

Configuration	Boundary Condition	PBL Scheme + Urban Canopy Scheme	Anthropogenic Inventory
BEP_MYJ	CAMS	MYJ + BEP	IER (5 km)
BEP_MYJ_CT	CarbonTracker		with hourly profile